Determination of hot workability and processing maps for AISI 904L stainless steel

Vroča preoblikovalnost nerjavnega jekla AISI 904L ter izračun procesnih map

Peter Fajfar[1,*], Boštjan Bradaškja[2], Boštjan Pirnar[2] & Matevž Fazarinc[1]

[1]University of Ljubljana, Faculty of Natural Sciences and Engineering, Aškerčeva 12, SI-1000 Ljubljana, Slovenia
[2]Acroni, Ltd., Research and Development, Cesta Borisa Kidriča 44, SI-4270 Jesenice, Slovenia

*Corresponding author. E-mail: peter.fajfar@omm.ntf.uni-lj.si

Received: November 8, 2011 **Accepted:** December 19, 2011

Abstract: Hot workability and microstructural evolution in dependence to deformation conditions for AISI 904L, super-austenitic stainless steel has been investigated on the basis of hot compression tests conducted on a thermo-mechanical simulator, Gleeble 1500D. Processing maps were calculated for various deformation conditions and correlated to the stability maps. An extensive microstructural analysis was conducted and a map of microstructures in correlation to deformation conditions was structured. This will all serve as a basis for better understanding of microstructural processes involved during the production of this steel.

Izvleček: S termomehanskim simulatorjem Gleeble 1500D sta bila preiskovana preoblikovalnost v vročem in razvoj mikrostrukture superavstenitnega nerjavnega jekla AISI 904L. Procesne mape in mape nestabilnosti so bile preračunane za različne stopnje deformacije, prav tako je bila izdelana tudi karta mikrostruktur v odvisnosti od preoblikovalnih parametrov. Taka analiza se uporablja za boljše razumevanje mikrostrukturnih procesov, ki se pojavljajo med vročim preoblikovanjem preiskovanega jekla.

Key words: AISI 904L stainless steel, processing maps, hot workability, hot compression testing
Ključne besede: nerjavno jeklo AISI 904L, procesne mape, preoblikovalnost v vročem, tlačni preizkusi v vročem

Original scientific paper

Introduction

AISI 904L is a non-stabilized, low-carbon, high-alloy superaustenitic stainless steel. These types of austenitic stainless steels are known to have very high ductility, formability and exceptional toughness.[1–4] These characteristics are present through a wide temperature range as a result of a single phase structure.

Because of the excellent corrosion resistance AISI 904L is manly used in highly aggressive environments.[5, 6] It has a very good oxidation resistance and retains strength at elevated temperatures.[7] The widespread of use is limited by the production costs on account of high nickel and molybdenum content and can reach high prices on the market compared to similar stainless steels. Thus the knowledge about the processes involved during hot deformation is of a great importance to minimize the processing costs and optimize the processing parameters and insure the uniform characteristics of the end product. The literature overview has shown that no studies of its hot deformation behavior and microstructural evolution during hot deformation were conducted.

The goal of this study was to investigate the hot workability and microstructural evolution during hot deformation, as a basis for process optimization and better understanding of the microstructural processes involved during production of this steel. The uniaxially deformed specimens were metallographically examined using light optical microscopy (LOM).

Gathered data from the experiments was used to calculate the processing maps for different logarithmic deformations and coupled with instability, which can be used in correlation with the microstructure maps to determine the optimal processing parameters during the production of this steel grade.

Materials and methods

The material used in this study is superaustenitic stainless steel AISI 904L. The higher content of copper in the AISI 904L enhances its corrosion resistance to strong reducing acids, e.g., sulphuric acid. Cylindrical specimens with an initial diameter of 8 mm and a height of 12 mm were machined from a 20-mm-thick, rolled, annealed plate, with its chemical composition listed in Table 1.

Table 1. Chemical composition of the AISI 904L stainless steels in mass fractions, (*w*/ %)

	C	Cr	Ni	Si	Mn	Mo	N	Cu	P	S
AISI 904L	0.0074	19.45	23.31	0.25	1.56	4.19	0.069	1.41	0.019	0.001

A computer-controlled, Gleeble 1500D thermo-mechanical simulator was used for the hot, uniaxial, isothermal compression tests. To reduce the friction between the specimen and the tool, and to avoid their mutual welding, a graphite lubricant foil and a 0.05 mm tantalum foil, respectively, were used. The temperature was measured at the central part of the specimen, using a spot-welded S-type thermocouple.

The testing was performed in the temperature range between 850 °C and 1 200 °C in 50 °C steps and at five different strain rates (0.001 s^{-1}, 0.01 s^{-1}, 0.1 s^{-1}, 1 s^{-1} and 5 s^{-1}). The specimens were heated to 1 200 °C with a heating rate of 10 K/s, followed by a 5 min soaking time at 1 200 °C. The temperature was subsequently lowered at 3 K/s to the deformation temperature, where it was held for another 5 min before deformation. The maximum true strain was set to 0.9. After the deformation the specimens were rapidly quenched into water (quench time <1 s).

True stress vs. logarithmic strain curves were calculated, taking into account the heat generated due to the high strain rates. The temperature rise was compensated for by applying the method proposed by Liu et al. [9]

The deformed specimens were cut along the mid-plane and metallographically prepared by grinding, polishing and electrolytic etching. Light optical microscopy was used to observe the microstructural features in each sample.

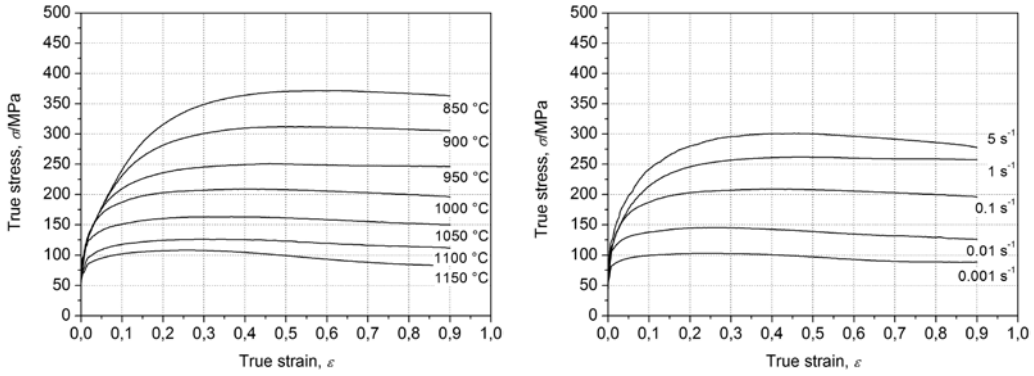

a) b)

Figure 1. True stress vs. strain curves for the AISI 904L material deformed a) with strain rates of 0.1 s^{-1} and b) at 1 000 °C.

RESULTS AND DISCUSSION

Compression tests

Typical true stress vs. trues strain curves are presented in Figure 1 for strain rates of 0.1 s^{-1} and deformed at 1 000 °C, respectively. After the initial deformation hardening, softening behavior occurs. It is attributed to dynamic recrystallization (DRX), which was later on confirmed by microstructural analysis. The flow curves of the tests performed at higher temperature and lower strain rates (Figure 1a) show steady state behavior after initial softening. This effect is not present at the flow curves of samples deformed below 1 100 °C and at higher strain rate than 1 s^{-1}.

Processing maps

With the use of data, gathered during compression tests, processing maps were calculated and the windows of instable deformations were calculated. Processing maps are developed on the basis of a dynamic material model (DMM) which has been suggested and widely used by the group of Prasad. [10–11] The processing maps of the material can be described as an explicit representation of its response to the imposed process parameters. It is a superimposition of the efficiency of power dissipation and an instability map.

The work-piece under hot deformation conditions works as an essential energy dissipater for this model. The constituent equation describes the manner in which energy (P) is converted at any instant into two forms, thermal energy (G) making temperature increase and microstructural change caused by transform of metallurgical dynamics (J), which are not recoverable. In general, most of the dissipation is due to a temperature rise and only a small amount of energy dissipates through microstructural changes. The power partitioning between G and J is controlled by the constitutive flow behavior of the material and is decided by the strain rate sensitivity (m) of flow stress as shown in the equation

$$\frac{\mathrm{d}J}{\mathrm{d}G} = \frac{\dot{\varepsilon}\,\mathrm{d}\sigma}{\sigma\,\mathrm{d}\dot{\varepsilon}} = \frac{\dot{\varepsilon}\,\sigma\,\mathrm{d}\ln\sigma}{\sigma\,\dot{\varepsilon}\,\mathrm{d}\ln\dot{\varepsilon}} \approx \frac{\Delta\lg\sigma}{\Delta\lg\dot{\varepsilon}} = m \quad (1)$$

where ε is true deformation, σ is true stress and $\dot{\varepsilon}$ is strain rate. For an ideal dissipater it can be shown that both quantities J and G are equal in their amount, which means that $m = 1$ and $J = J_{max}$ whereas the efficiency of power dissipation η is given by:

$$\eta = \frac{J}{J_{max}} = \frac{2m}{m+1} \quad (2)$$

The variation of power dissipation with temperature and deformation represents the relative value of energy dissipation occurring through microstructural changes. Microstructural changes, which include a dynamic recovery and dynamic recrystallization, are desired and values for efficiency of

power dissipation η are in such cases in range 0.3–0.4. Lower values for η are less desired and often overlap with area of instable hot deformation (described bellow). Thus lower values for η refer to wedge cracking, void formation at hard particles, dynamic strain ageing and intercrystalline cracking, etc. High values of η refer to formation of new surface related to microcracking.

The instability map is defined by a stability criterion for a dynamic material, where the differential quotient of its dissipative function has to satisfy an inequality condition (ζ), given by equation 3, to allow a stable flow.

$$\xi\left(\dot{\varepsilon}\right) = \frac{\partial \ln(m/(m+1))}{\partial \ln \dot{\varepsilon}} + m > 0 \qquad (3)$$

Areas with values for $\zeta < 0$ are considered as non-stable for hot deformation. These areas refer to adiabatic shear bands, flow localization, Lüder's bands, etc.

The maps, calculated for deformations of 0.1, 0.2, 0.4 and 0.6 are presented in Figure 2. They were calculated for the processing parameters applied during compression tests; for temperature range from 850 °C to 1 150 °C and strain rates 0.001 s^{-1} to 5 s^{-1}. The dissipation maps are similar at various strains. The instable zone with $\zeta < 0$ (gray region) starts forming at deformation 0.1 in the temperature region around 1 050–1 100 °C, and strain rate of around 0.1 s^{-1}. The instability region grows with the raise of deformation, covering a processing area of strain rates from around 0.01 s^{-1} to 1 s^{-1} and temperature range from 1 000 °C to 1100 °C. This processing area should be avoided; strain rates have to be high enough.

From Figure 2 it is clearly seen that instability area overlaps with area with high value for η that although indicates on safe hot forming.

Microstructural analysis

Microstructures of deformed specimens were inspected in the center part of the specimen where the highest deformation was present during compression. The comparison of initial microstructure and the microstructure before deformation is presented in Figure 3. The initial microstructure shows a very evenly distributed, recrystallized microstructure with recrystallization twins present. The measured mean grain size was ≈80 μm. As expected, the grains had grown substantially in the pre-deformation heating stage. This is contributed to the minimization of surface energy through the increase of the grain size. The austenite grains contain annealing twins which are characteristic for the alloys with low stacking fault energy.

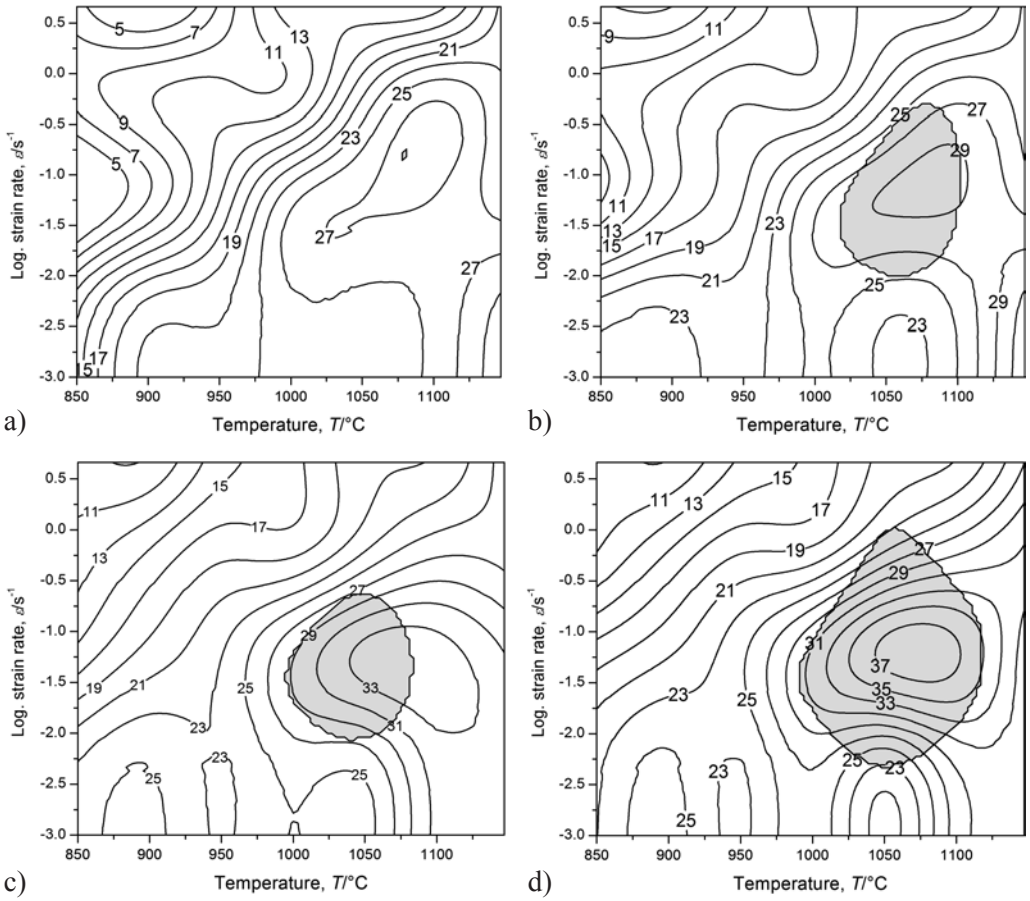

Figure 2. Processing maps for AISI 904L stainless steel, at strains a) $\varepsilon = 0.1$, b) $\varepsilon = 0.2$, c) $\varepsilon = 0.4$ and d) $\varepsilon = 0.6$.

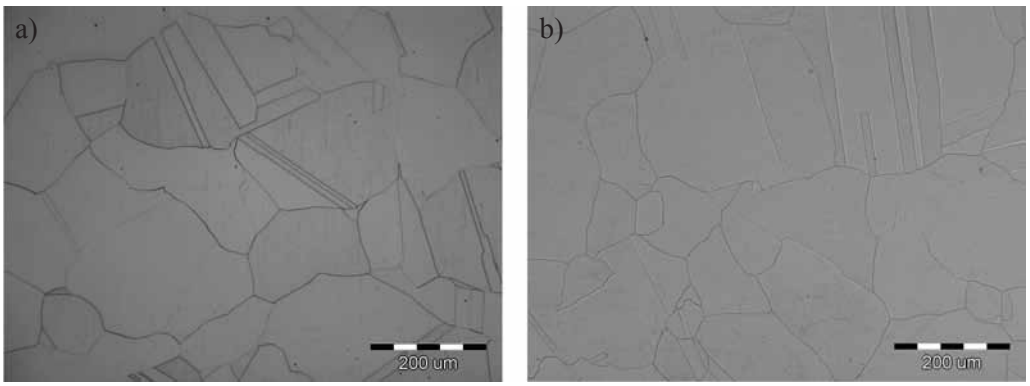

Figure 3. Microstructure of AISI 904L-stainless steel. a) as-received state, b) after soaking at 1 200 °C for 5 min and subsequent water quenching.

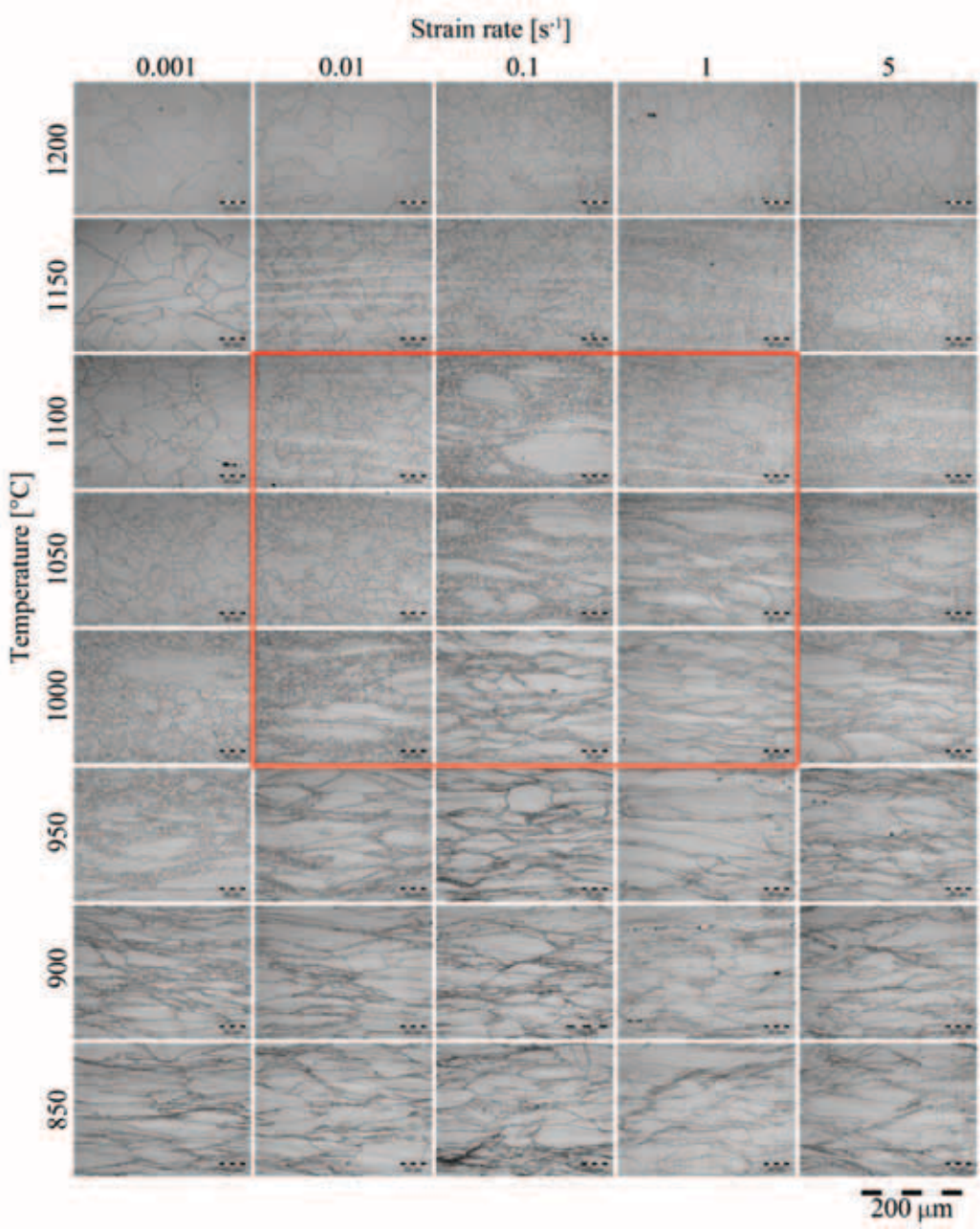

Figure 4. Obtained microstructures after deformation at various strain rates and temperatures. Quenched after deformation to $\varepsilon = 0.9$.

The microstructural map, presented in dependence to processing parameters is presented in Figure 4. No recrystallized grains are to be found in the specimens deformed with higher strain rates (1 s^{-1} and 5 s^{-1}) and below 950 °C. On the other hand, other specimens did recrystallize some partly, with only necklace type microstructure, with small recrystallized grains around deformed larger grains and some fully recrystallized. Appearance of necklace type microstructure indicates that DRX was not completed. The DRX necklace which follows dynamic nucleation usually takes place in a coarse-grained structure under deformation at low temperature or high strain rates.

The region, marked with red border, shows the region where instability maps predicted low microstructural stability. It can be seen that the grain size is widely distributed, from very small recrystallized grains in necklace to large deformed primary grains. This could cause unstable deformation and as such should be avoided during processing.

Conclusions

Hot deformation behavior of AISI 904L-stainless steel was studied, using thermo-mechanical processing. From the gathered results, the following conclusions can be drawn:

- After initial deformation hardening, softening mechanisms are observed, and steady state flow stress is achieved at the logarithmic strain of 0.9 below the strain rate of 1 s^{-1} and above 1 100 °C.
- Processing maps, calculated on the basis of compression test show an instability region below 1 s^{-1} and between 1 000 °C and 1 100 °C.
- Microstructural analysis showed a gradual increase of dynamically recrystallized material with a decrease of strain rate and increase of temperature. A fully recrystallized microstructure is found in specimens deformed with a strain rate of 0.001 s^{-1} and above 1 050 °C.
- The comparison between results of the map of microstructural evolution and the processing maps are in good agreement, providing useful information for process guidance.
- Highest values for efficiency of power dissipation were obtained around 1 050 °C and strain rate of 0.1 s^{-1}.

References

[1] Belyakov, A., Miura, H. & Sakai, T. (1998): Dynamic recrystallization under warm deformation of a 304 type austenitic stainless steel, *Material Science and Engineering, A*, 255, pp. 139–147.

[2] Deghan-Manshadi, A., Barnett, M.

R. & Hodgson, P. D. (2008): Recrystallization in AISI 304 austenitic stainless steel during and after hot deformation, *Material Science and Engineering, A*, 485, pp. 664–672.

[3] Fréchard, S., Redjaïmia, A., Lach, E. & Lichtenberger, A. (2008): Dynamical behavior and microstructural evolution of a nitrogen-alloyed austenitic stainless steel, *Material Science and Engineering, A*, 480, pp. 89–95.

[4] Nemat-Nasser, S., Guo, W. G. & Kihl, D. P. (2001): Thermo-mechanical response of AL-6XN stainless steel over a wide range of strain rates and temperatures, *Journal of Mechanical Physics of Solids*, 49, pp. 1823–1846.

[5] Moayed, M. H. & Newman, R. C. (2006): Deterioration in critical pitting temperature of 904L stainless steel by addition of sulfate ions, *Corrosion Science*, 48, pp. 3513–3530.

[6] Iversen, A. K. (2006): Stainless steels in bipolar plates—Surface resistive properties of corrosion resistant steel grades during current loads, *Corrosion Science*, 48, pp. 1036–1058.

[7] Laycock, N. J. & Newman, R. C. (1998): Temperature dependence of pitting potentials for austenitic stainless steels above their critical pitting temperature, *Corrosion Science*, 40, pp. 887–902.

[8] Stauffer, A. C., Koss D. A. & McKirgan, J. B. (2004): Mechanical Behavior - Microstructural Banding and Failure of a Stainless Steel, *Metallurgical and Materials Transaction: A*, 35A, pp. 1317–1324.

[9] Liu, J., Chang, H., Wu, R., Hsu, T. Y. & Ruan, X. (2000): Investigation on hot deformation behavior of AISI T1 high-speed steel, *Materials Characterization.,* 45, pp. 175–186.

[10] Prasad, Y. V. R. K., Sasidhara, S. (1997): *Hot Working Guide, Compendium of Processing Maps*, ASM - International, OH, USA, 1997, pp. 1–24.